

Effect of cavity design on textured tool surfaces in sheet metal forming

Philipp Schumann^{*,*}, Daniel Martin^{*}, Otavio Moro Serra^{*}, Mano Prithvi Raj Raja^{*}, and Peter Groche^{*}

Institute for Production Engineering and Forming Machines (PtU), Technical University of Darmstadt, 64287 Darmstadt, Germany

Received: 29 August 2025 / Accepted: 25 October 2025

Abstract. In order to advance sustainability in manufacturing, it is necessary to reduce both energy use and material waste. Tribology is recognised as a central factor in this effort. In sheet metal forming, for example, friction and wear lead to increased energy demand, tool degradation and lubricant consumption. Therefore, surface texturing has emerged as a promising strategy to improve tribological efficiency, contributing to both technical performance and reduced environmental impact. Building on earlier findings which identified cavity geometry, spatial distribution and load conditions as decisive parameters, this study introduces a systematic methodology for designing surface textures for lubricated forming operations. Computational fluid dynamics is used to analyse the rheological mechanisms underlying lubricant flow and pressure generation in textured interfaces. The optimal cavity design is defined by its ability to minimise the coefficient of friction. The results demonstrate that lubricant reservoirs and hydrodynamic pressure formation depend heavily on cavity dimensions and distribution. In particular, the coverage ratio and lubrication clearance are shown to have the most significant influence on friction reduction. These insights pave the way for more resource-efficient and sustainable sheet metal forming processes by linking tribological performance to reduced energy demand and extended tool life.

Keywords: Micro texturing / CFD / tribology / cavity design

1 Introduction

Industrial manufacturing processes account for 15% of global energy consumption and between 35–40% of global material use [1]. This disproportionately high share is attributable to the sustained and expanding demand for sheet metal products, particularly within the housing and automotive sectors, constituting two of the most resource-intensive domains of modern economy. Forecasts indicate that worldwide energy consumption will increase by nearly 20%, rising from 584 exajoules in 2019 to approximately 700 exajoules in 2040. This trend is primarily attributable to global population growth, increasing demand for consumer goods, and accelerated product development cycles characterized by reduced lifespans [2,3]. Meeting these energy requirements while achieving internationally agreed climate objectives necessitates not only the substitution of fossil fuels with renewable energy carriers but also substantial

improvements in industrial efficiency [4]. The optimization of existing value chains has been identified as a central strategy for sustainable development [5].

Tribological losses represent a particularly significant contributor to global energy demand. It is estimated that friction and wear account for nearly 23% of primary energy consumption when considering the entire value chain, including raw material extraction, processing, energy production, and transportation [6]. In parallel, regulatory frameworks such as the Agenda 2030 [7] and the REACH regulation [8], as well as strategies aligned with the 3R principle (reduce, reuse, refine) [9], are reshaping industrial production through stricter controls on CO₂ emissions and environmentally harmful substances. Within this context, insufficient tribological performance results in elevated energy consumption, premature component degradation, and increased maintenance costs, thereby posing significant technical and economic challenges [10]. These issues are particularly evident in the sheet metal forming sector, where friction and lubrication determine not only product quality and process productivity but also the environmental performance of manufacturing systems [11]. Consequently,

* e-mail: philipp.schumann@ptu.tu-darmstadt.de

* These authors contributed equally to this work.

the enhancement of tribological properties offers considerable potential for both energy and resource efficiency [12]. The most significant can be summarized as:

- Reduction of friction.
- Reduction of material footprint, achieved through:
 - Extended component lifetime due to lower wear and fatigue.
 - Reduced lubricant consumption und environmental benefits.

These potentials lead to an enormous research opportunity for the improvement of tribological properties. One of the most promising approaches to realising the potentials listed above is micro texturing. Surface modification is well established across multiple technical domains due to beneficial effects on the coefficient of friction (COF) and increasing service life. Textures can be classified according to scale in three principal categories: meso-; micro- and nano-level textures. The conceptual foundation of surface micro-texturing is rooted in biomimetic design, inspired by natural systems such as shark skin, which exhibits pronounced drag-reducing capabilities during hydrodynamic locomotion [13]. Within manufacturing applications micro texturing has emerged as a promising approach. For sheet metal processes various studies were performed, investigating the resulting effectiveness of the surface modification.

As previously proposed by Yang et al. [14] transferring and implementing proven technologies has the potential to significantly improve the resource and energy efficiency of industrial processes, thereby making a significant contribution to decarbonisation. As demonstrated by numerous applications in industry and literature, deterministic texturing of surfaces can significantly improve the tribological performance of manufacturing processes by inhibiting adhesive and abrasive wear [15]. The approach is mainly used to modify the surfaces of tools. Texturing notably improves the life of turning inserts [16]. Hazrati et al. significantly reduced friction and the required punch force for deep drawing and bending by texturing distinct areas of the punch [17]. Shimizu et al. [18] demonstrated, that surface texturing contributes to a reduction of the COF in a deep drawing process. Kitamura et al. [19] and Schumann et al. [20] observed reduced process forces when using blanking punches with different texturing approaches. Experimental observations showed that the structures applied to cutting dies significantly improved wear behaviour and increased service life. Kersting et al. demonstrated similar effects investigating various textures in experiments for tribological loads in sheet-bulk metal forming. Using ring-compression and pin-extrusion tests, friction coefficients for the textures were acquired. Subsequent forming simulations showed improved form-filling and reduced process forces [21].

Numerous studies have repeatedly demonstrated that variations in texturing parameters – such as the geometry of individual features, the coverage ratio and the orientation – can exert either beneficial or detrimental effects on tribological performance. With regard to the cover ratio, it has been shown that friction is reduced with increasing coverage up to approximately 18%, however, beyond a

threshold of 20% an abrupt rise in friction is observed [17]. The specific forming process and the prevailing tribological load conditions are therefore decisive factors in determining whether surface texturing enhances or impairs performance. The leading trial and error analyses for investigating and optimizing textures are not only time-consuming and costly, but they also yield limited insight into the underlying mechanisms responsible for positive tribological effects. Consequently, a systematic design methodology is essential for targeted development of functional textures. Hence, Uehara et al. [22] postulated a direct correlation between coverage ratio and the coefficient of friction. While this fundamental relationship is widely accepted, subsequent investigations have shown that variations in the applied load spectrum may shift the optimum coverage ratio relative to the initially proposed value [23].

Ciulli et al. [24] highlighted how tribological strategies contribute to the achievement of sustainability targets set forth by the European Parliament. Their work underscores that systematic microtexture design constitutes an effective means of advancing the geopolitically motivated objective of maximizing energy efficiency across a wide range of industrial processes and load scenarios. The literature has already shown that simulations based on computational fluid dynamics (CFD) are a resource-efficient tool for simulating and analysing the fluid mechanical effects that occur. Liu et al. [25] and Tomic et al. [26] confirmed the suitability of CFD models for describing texturing behavior through qualitative comparisons with experimental results. Nevertheless, unlike the novel modelling approaches developed by Caretta et al. [27], conventional CFD approaches do not account for plastic deformation and are restricted to hydrodynamic lubrication regimes, primarily for reasons of computational efficiency. Moreover, spatial variables are generally reduced to a two-dimensional representation. Combined, these results provide a conceptual foundation for a generalized and systematic approach to texture and cavity design.

Against this background, the present study uses a CFD-based methodology to investigate optimal texture configurations for various sheet metal forming applications. The aim is to enhance energy efficiency, cost-effectiveness and material utilisation while facilitating the in situ observation and analysis of relevant rheological phenomena.

2 Material and methods

Texturing tribologically interacting surfaces can substantially improve the performance of forming processes. However, the degree of improvement depends heavily on the characteristics of the tribological system, the load spectrum and the geometry and density of the applied cavities. This implies that specific forming processes require distinct surface textures. In order to develop a systematic and targeted design methodology, the present study investigates the influence of key parameters across different tribological load collectives. The strip drawing test is employed as a reference method for comparative

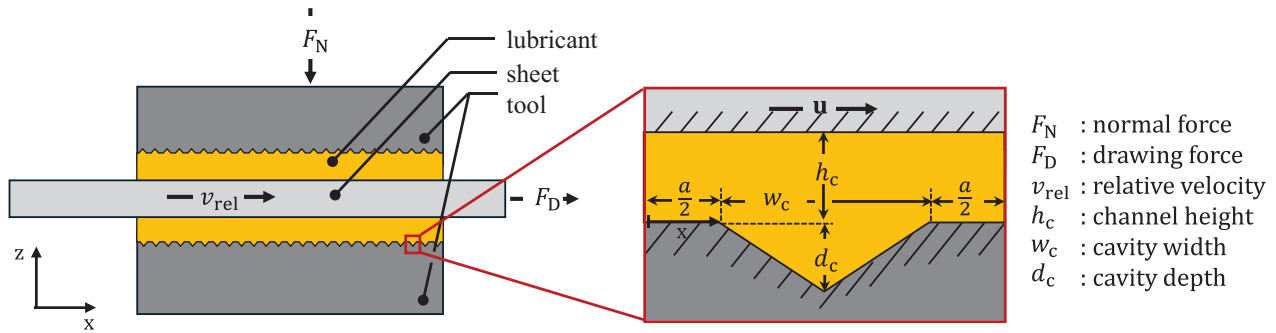


Fig. 1. Physical set-up of the tribometer and geometrical abstractions.

evaluation, enabling system- and process-related variations to be isolated and facilitating relative comparisons with prior experimental studies. Within this framework, three representative cavity geometries, selected for their manufacturability, are examined. We propose a computationally efficient approach to assessing the effectiveness of texturing prior to experimental validation by introducing novel geometric abstraction techniques for estimating the coverage ratio. This publication builds upon the findings of Schumann et al. [28], extending the analysis of cavity shape effects on friction reduction and benchmarking the computational predictions against experimental results.

2.1 Tribological system

This study focuses on the tribological performance of textured surfaces in sheet metal forming. The strip drawing test is a well-established method to characterise the frictional behaviour of tribological systems in sheet metal forming. Tools with simple geometry are used to simulate different tribological loads of the abstracted process. This facilitates the validation for future investigations as technical variables can be varied in isolation [29]. Thanks to the minimised geometric setup of this analogue experiment and the ability to adjust the isolated variables of the tribological load collective, such as the normal force, this setup is ideal for evaluating textured surfaces. It also provides an optimal foundation for the subsequent transfer to a two-dimensional computational fluid dynamics (CFD) simulation. Figure 1 shows the schematical model of the experimental test and the extracted section that was used for the design of the CFD model.

The characterization of microtextured surfaces is conducted using the continuous strip drawing test introduced by Groche et al. [30]. This experimental setup is designed to replicate characteristic load conditions encountered in sheet metal forming operations. The use of interchangeable die inserts enables systematic evaluation of different surface textures. The die inserts used allow various surface textures to be tested. The individual inserts have a square shape with length of 40 mm, rounded edges, and their modular design allows for efficient replacement, thereby ensuring compatibility with extended test series. Within the test series individual sheet metal strips are used, enabling repeatable testing procedures.

In the test stand, the required normal force F_N is applied via four hydraulic cylinders. After closing the dies and applying the specific load the drawing force F_D is induced to the sheet by a drawing mechanism. Each stroke has a length of 100mm, with a controlled drawing velocity of $100 \frac{\text{mm}}{\text{s}}$. This configuration permits the generation of load collectives that closely reproduce the stresses and strains characteristic of industrial sheet metal forming processes, thus facilitating systematic and large-scale investigations [31]. The lubricant was applied automatically immediately before the strip drawing stage using precision valves from Raziol. This ensured robust reproducibility across the entire test series. The quantity of lubricant was calibrated in advance using a precision scale from Kern while investigating several sheet metal strips. The resulting coefficient of friction (COF) is then computed according to the following relation:

$$\mu = \frac{F_D}{2 \cdot F_N}. \quad (1)$$

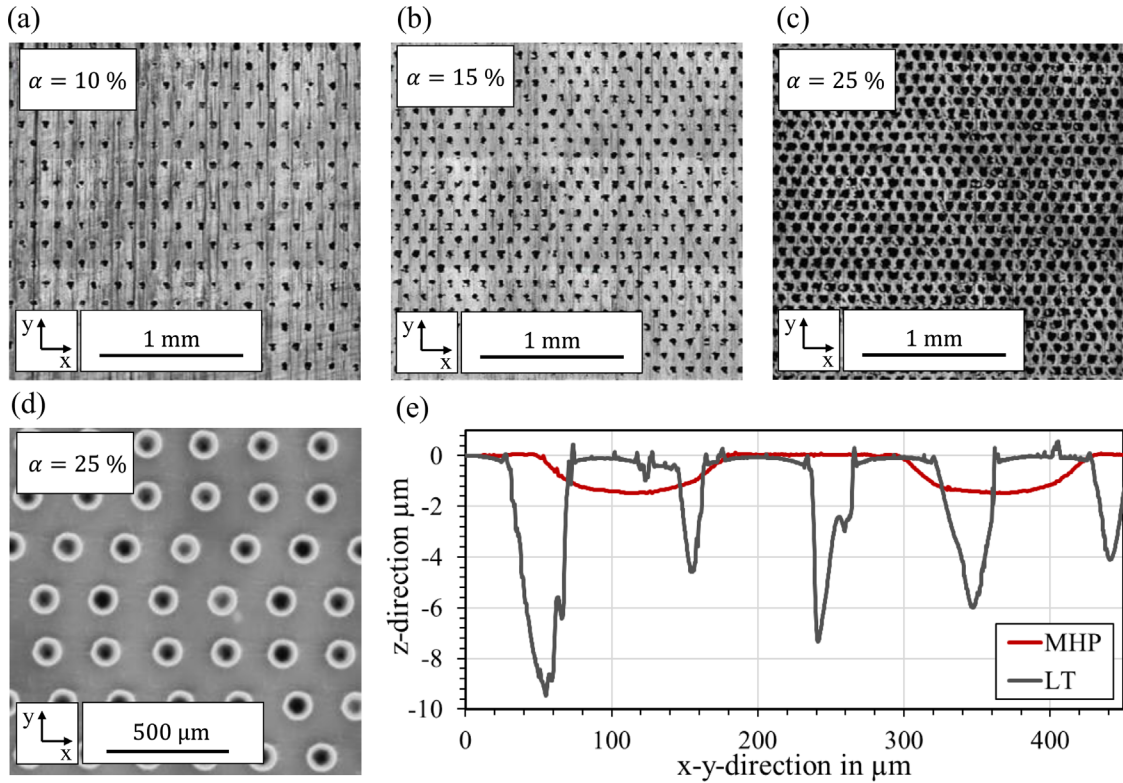
The tribological system used as a reference for the experimental set up and simulation is described in Table 1.

2.2 Textured surfaces

As previous work of the authors introduced the frictional behaviour, the dies can be influenced using laser texturing (LT) and machine hammer peening (MHP) [23]. For LT, a pulsed, frequency-doubled nanosecond laser from 3D micromac is used. In contrast, texturing by MHP is performed using an electromechanical system provided by accurapuls, coupled with a conventional CNC machine serving as the positioning manipulator. Therefore, a microturned microtip on top of the peening head embosses cavities on the machined surface. The detailed process kinematics and associated effects are documented in previous work by the authors [20]. The spacing between the individual cavities was chosen to be equidistant, such that the ratio between the total projected area covered with cavities – referred to as coverage ratio α – can be systematically adjusted. Specifically, α is controlled by varying the center-to-center spacing a between individual cavities, α . Under the assumption of deterministically distributed, cylindrical cavities of diameter w_c , arranged in

Table 1. Tribological system experimentally investigated.

Tool		Sheet			Lubrication		
Material	Hardness h in HRC	Material	Thickness s in mm	Strength R_m in MPa	Type	Amount g in $\frac{g}{mm^2}$	Viscosity θ in mm
1.2379	60	HC420LA	1.5	530 ± 60	RhenusSU	1	200

**Fig. 2.** Topographies of the (a)-(d) laser textured; (d) MHP textured surfaces and the intersection of the cavities.

a periodically repeating pattern along the x - and z -direction with a spacing a , the coverage ratio can be expressed as follows:

$$\alpha = \frac{\pi \cdot w_c^2}{4 \cdot a^2}. \quad (2)$$

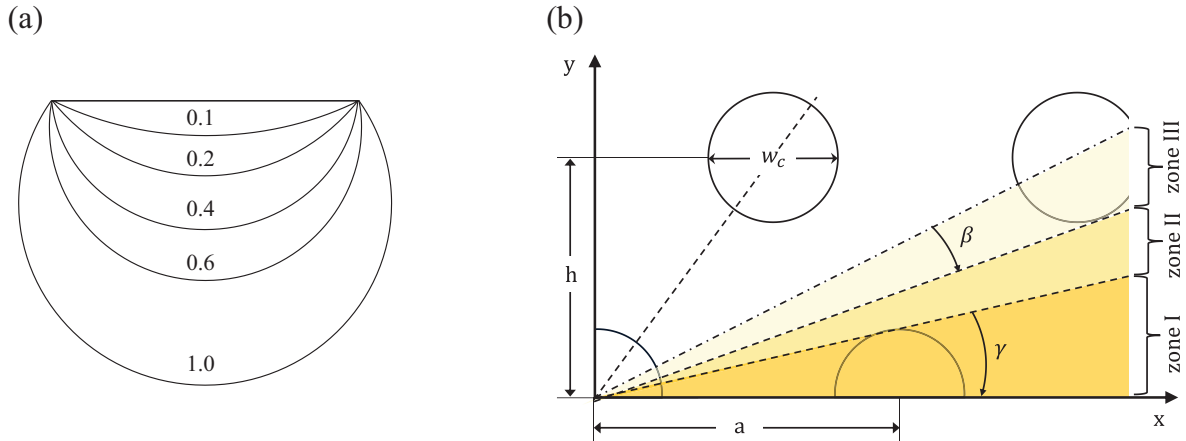
The smallest repeating texture element is defined as an isosceles triangle with a leg angle of 60° . One of the most fundamental distinctions between the two processes under consideration lies in their respective material utilisation mechanisms, beyond the resulting cavity geometries. LT is a material-removal technique based on localised thermal effects, whereas MHP relies on the plastic deformation of the base material. Consequently, the MHP approach notably enhances material efficiency. In addition, it has been shown that the plastic deformation induced by MHP generates secondary effects, including cold work hardening and the induction of compressive residual stresses at the surface. These phenomena are generally recognised as being beneficial to the tool's operational lifetime. However,

MHP also subjects the microtip of the peening head to substantial mechanical loading, accelerating wear when machining hardened tool steels. For this reason, only one set of tools was textured using MHP in the strip drawing experiments. In contrast, LT results in the partial resolidification of ablated material on the surface. This necessitates an additional post-processing polishing step to achieve the desired finish. This requirement does not apply to MHP. Confocal microscopy was employed to characterise and validate the generated surface topographies. The confocal microscope used is a Surf expert by NanoFocus AG, which is equipped with a 20 x magnifying lens. The surfaces considered for verification of the simulation are shown in [Figure 2](#).

[Figure 2e](#) shows intersections of the generated cavities. This illustrates the difference in the shape and dimensions of the textures. While LT generated conical cavities, those created by MHP have a spherical shape. The tool pairs considered for the experiment and their surface properties are listed in [Table 2](#). The textured strip drawing dies are compared with a conventional polished die having a roughness of $Rz = 32.2 \pm 0.6 \text{ nm}$ and $Ra = 3.5 \pm 0.3 \text{ nm}$.

Table 2. Cavity parameters generated by different manufacturing processes.

Specimen	Process	Shape	α in %	w_c in μm	d_c in μm	A_R
LT ₁₀	LT	Conical	10	50 ± 8.3	5.90 ± 1.5	0.1
LT ₁₅			15			
LT ₂₅			25			
MHP ₂₅	MHP	Spherical	25	130 ± 2.1	1.5 ± 0.1	0.01

**Fig. 3.** (a) Schematic representation of aspect ratio A_R for spherical cavities and (b) geometrical assumptions for cavity spacing a based on coverage ratio α .

Three versions of each pair were produced and examined. Due to severe wear on the micro tip when machining the die surfaces, only one pair could be produced using MHP.

3 Computational fluid dynamics

3.1 Geometrical setup

It has been shown that the tribological beneficial mechanisms of textured surfaces depend on the lubrication system. Under hydrodynamic lubrication, the improvement in load carrying capacity is the main mechanism that can be impacted through the manipulation of topography, an can thereby be reflected in numerical simulations. Considering the feasibility of the observed phenomena to process applications, the CFD model was designed as an abstraction of the strip drawing test referenced. Relevant geometric parameters for describing the interdependencies of the cavities experimentally applied in 2-dimensional space are visualised in Figure 1. Another parameter that has been found to significantly influence tribological performance is the aspect ratio A_R , which can be determined as follows:

$$A_R = \frac{d_c}{w_c}. \quad (3)$$

Figure 3a shows a geometrical representation of different aspect ratios when assuming a spherical cavity shape. Numerous studies identified the surface coverage α as a critical parameter governing the tribological performance of textured surfaces [22]. Accordingly, the coverage

ratio defined in equation (2) must also be incorporated into the simulation framework. For the CFD simulations of textures previously applied in experimental studies, several simplifying assumptions were introduced to facilitate the projection of the texturing pattern and the corresponding coverage ratio in the x-z plane [19]. Based on a line spacing h , which contributes to the creation of isosceles triangles between the indentations, the distribution is described trigonometrically. Starting from a single cavity, the projected distances to the nearest surrounding cavities in radial propagation around the cavity under consideration were mathematically averaged. This assumption yielded the three characteristic zones visualized in Figure 3b.

Based on these assumptions, an analytical approximation is made for the cavity spacing a , as a function of coverage ratio α .

$$\frac{a}{w_c} = -1 + \frac{1}{\gamma + \beta} \left(2 \int_0^\gamma \sqrt{1 - A^2 \sin^2 \theta} d\theta - \int_0^\beta \sqrt{1 - 3A^2 \sin^2 \theta} d\theta \right) \quad (4)$$

where:

$$A = \sqrt{\frac{2\pi}{\sqrt{3\alpha}}} \quad (5)$$

$$\gamma = \arcsin\left(\frac{1}{A}\right) \quad (6)$$

$$\beta = \min \left\{ \arcsin \left(\frac{1}{\sqrt{3A}} \right), \frac{\pi}{6} - \gamma \right\}. \quad (7)$$

Considering the zones introduced in [Figure 3](#) and the possible solutions to the equations, a calculated limit of 40.1% results for the two-dimensional simulation case. In the three-dimensional view, the arrangement resembles a face-centered cubic unit cell. Thus, the calculated limit without texture overlaps for this case is 90.68%. A large number of experimental studies already showed that texturing up to max 35% has a positive effect on the friction properties [[19,32–34](#)]. This means that the chosen simplification is still suitable for a basic assessment of the effectiveness of different textures.

3.2 Governing equations

The numerical framework employed in this study is based on the fundamental conservation laws governing fluid motion, thus assuming the continuity equation and the Navier-Stokes equations for an incompressible Newtonian fluid treated as a continuous phase medium.

$$\nabla \cdot \mathbf{u} = 0 \quad (8)$$

$$\rho \left(\frac{\partial \mathbf{u}}{\partial t} + (\nabla \cdot \mathbf{u}) \mathbf{u} \right) \cdot \mathbf{u} = -\nabla p + \vartheta \nabla^2 \mathbf{u}. \quad (9)$$

In this formulation, ρ is the density of the lubricant, \mathbf{u} is the velocity vector field, p the static pressure and ϑ the dynamic viscosity of the fluid. The assumption of Newtonian behaviour implies a linear relationship between shear stress and shear rate, which is commonly adopted for lubricants under moderate operating conditions. In the present model, potential variations in viscosity arising from piezo-viscous effects (i.e. changes in viscosity dependent on pressure) or rheological effects such as shear-thinning or non-Newtonian behaviour are neglected. This simplification is justified by the fact that lubricants can be reasonably approximated as Newtonian fluids for the majority of metal forming applications at moderate pressures and shear rates [[35–37](#)]. However, it should be acknowledged that under extreme contact pressures or elevated temperatures, lubricants may deviate from Newtonian characteristics, which could lead to localised discrepancies between numerical predictions and experimental results.

3.3 Boundary conditions

The relative motion of the triboelements in contact was simulated by imposing a constant velocity condition on the upper wall, $y = h_c$, where the lubrication clearance h_c is equal to the film thickness. Flow was assumed to be periodic with a repeating unit consisting of one cavity. Periodicity is imposed using OpenFOAM's native cyclic setting, which initialises the fields at those faces to be equal to the internal initial condition, and employs periodicity to calculate them at every subsequent iteration. Therefore, all

fluid fields are constrained to have the same values at the inlet and outlet. The lower wall, corresponding to the microtextured element, was modelled as a no slip boundary condition, along with a zero-gradient condition for the pressure field. A preliminary convergence analysis showed that a time step of $\Delta t = 10^{-8}$ s and a grid size of $0.1 \mu\text{m}$ are suitable.

3.4 Performance parameters

In line with the approach proposed by Liu et al. [[25,38](#)], performance parameters have been introduced in order to evaluate the tribological behaviour of the model. Denoting p as the hydrodynamic pressure and τ as the shear stress distribution function, the drag force F_d and lift force F_L over the moving wall are subsequently calculated as follows:

$$F_d = \int \tau dx \quad (10)$$

$$F_L = \int p dx \quad (11)$$

Incorporating the characteristic length L the drag c_d and lift coefficient c_l can be computed:

$$c_d = \frac{F_d}{\frac{1}{2} \rho u^2 L} \quad (12)$$

$$c_l = \frac{F_L}{\frac{1}{2} \rho u^2 L} \quad (13)$$

Where u is the sliding speed and L the length of the upper tool part simulated (see [Fig. 1](#)). The friction coefficient COF is instead computed in relation to the external force F_L :

$$\mu = \frac{F_d}{F_L}. \quad (14)$$

If μ_0 refers to the friction of a smooth, untextured surface under the same boundary conditions, then the relative change in friction is computed as a percentage:

$$\Delta\mu = \left| \frac{\mu - \mu_0}{\mu_0} \right| \cdot 100. \quad (15)$$

A higher friction reduction rate indicates an improved tribological performance of the sliding bodies.

3.5 Mesh generation

The two-dimensional meshes for the spherical and conical microtextures were generated using OpenFOAM's native *blockMesh* utility. To maintain a desirably uniform mesh with hexahedral cells, especially in the lubrication clearance, the meshes were parameterised. Parameterisation of the mesh also allows for variations based on lubrication clearance h_c , cavity depth d_c , and cavity

Table 3. Number of elements for fixed aspect ratio $A_R = 0.5$ and ($h = 3 \mu\text{m}$, $w_c = 10 \mu\text{m}$, $d_c = 5 \mu\text{m}$).

Mesh size in μm	Rectangular	Spherical	Conical
0.5	500	484	945
0.25	2000	1936	3780
0.20	3140	2760	6004
0.1	12500	11530	23625

width w_c . In the present study, the parameterisation is based on a fixed aspect ratio between the cavity depth and its width.

The number of cells depends on the geometry, the domain parameters, the aspect ratio and the mesh size (within the channel of the domain). The mesh is parameterised so that the smaller mesh size leads to smaller elements, and, therefore, a finer mesh. The aspect ratio A_R is calculated according to equation (4). The conical geometries have more cells than the rectangular and spherical geometries, due to the meshing strategy (C-grid for spherical dimples, Y-grid for conical dimples) implemented to generate structured meshes, while maintaining numerical stability. However, the resulting meshes contain a small number of non-orthogonal cells, which may impact stability of the solution. To address this issue, non-orthogonal correctors have been added to the PIMPLE loop in *system/foSchemes*. The resulting number of elements for different cavity shapes is shown in Table 3.

3.6 Mesh independence study

It is crucial that the simulation results do not vary significantly with increasing mesh refinement. While refining the mesh improves simulation accuracy, it also increases the computational effort. Therefore, it is necessary to find a suitable mesh size to obtain reasonable accuracy. This is done by starting with an initially coarse mesh size, monitoring a quantity of interest — in this case the drag coefficient c_d — and refining the mesh until this quantity no longer changes significantly.

In Figure 5, the effect of increasing mesh refinement on c_d is minimal. A mesh size in the intermediate range is recommended to ensure sufficient accuracy while maintaining reasonable computational cost, especially for complex cases like the spherical and conical micro-dimple textured surfaces. Therefore, the mesh size was set to $0.25 \mu\text{m}$.

3.7 Simulation procedure

The aforementioned parameters and assumptions were implemented in OpenFOAM v2012 by adapting the native cavitatingFoam solver. In the context of hydrodynamic lubrication, load carrying capacity is a key performance indicator as it reflects the tribological conditions at the contact interface. This parameter primarily depends on pressure distribution (see Eq. (11)) and can be extracted from the numerical results. To evaluate the influence of geometric texturing parameters on tribological

performance and determine their relative significance, systematic variations were introduced within the dimensional ranges previously investigated experimentally (see Sec. 2.1). This ensured the feasibility of the chosen assumptions. In particular, the influence of cavity depth d_c and aspect ratio A_R (see Eq. (3)) on pressure build-up and lubricant retention was examined. The process velocity was set to $\mathbf{u} = 100\text{mm/s}$, consistent with the experimental strip drawing tests. A full factorial design of experiments was employed, resulting in a comprehensive dataset of 576 simulations (see Table 4).

In addition, the influence of the cavity shape was investigated. Since mesh generation for cavities with a conical and spherical design is significantly more complex than for cavities with a rectangular profile, a different test matrix was designed for this analysis, which is shown in Table 5. Based on the findings of the parameter variation from Table 4, the lubrication clearance was set to $h_c = 1 \mu\text{m}$. The remaining model assumptions are as described above. This resulted in a total of 378 simulations. The performed numerical campaigns provide a robust basis for correlating texture geometry with hydrodynamic performance, as well as for guiding subsequent experimental validation.

4 Results and discussion

4.1 Relative frictional behavior of textured dies

The textured and polished die pairs were examined under the tribological system presented in Table 1, while the effective contact normal stress (CNS) was varied by increasing the normal force F_N . Figure 4a shows the recorded average friction coefficients for the tools examined over the entire sliding length.

To simulate different tribological load conditions, the effective contact normal stress was incrementally increased by increasing the normal force during each test series. Yang et al. observed a lubrication film thickness of $5 \mu\text{m}$ for similar stress states and viscosity for a deep drawing process [39]. The distribution of values is shown in a box plot in Figure 6b, and the mean values with corresponding standard deviation are shown in Figure 6c for the load intervals. Based on the results of the work presented, the relative change in the COF of textured surfaces compared to a conventional polished surface within a load level was determined from the friction coefficients determined in the investigations carried out. This corresponds formally to:

$$\Delta\mu_{\text{ex}} = \frac{|\mu_s - \mu_t|}{\mu_s} \cdot 100 \text{ for } \text{CNS} = \text{const.} \quad (16)$$

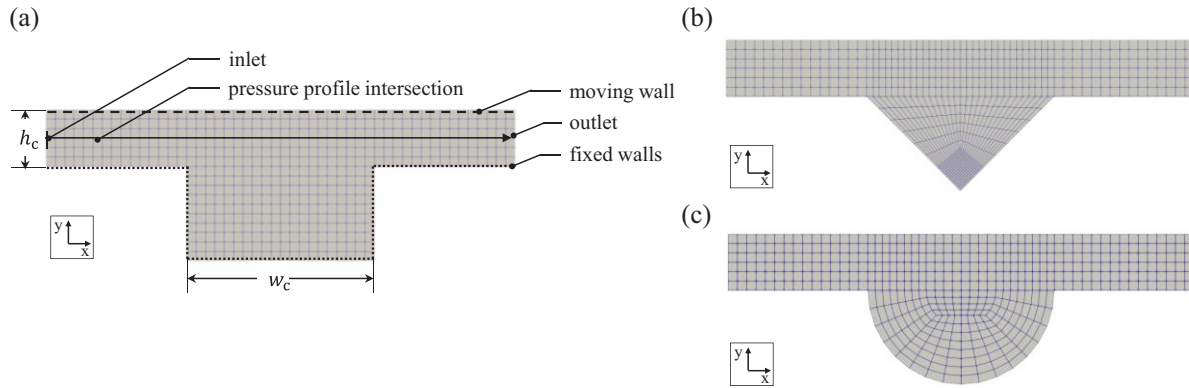


Fig. 4. Mesh of domain for different microtexture shapes (a) rectangular, (b) conical and (c) spherical for: $h = 3 \mu\text{m}$, $w_c = 10 \mu\text{m}$, $A_R = 0.5$.

Table 4. Parameters varied simulatively.

A_R [-]	h_c in μm	w_c in μm	α in %
0.01; 0.05; 0.1; 0.25	1; 5; 10; 50	10; 25; 50; 100; 150; 200	5; 10; 15; 20; 25; 30

Table 5. Parameters varied simulatively for the investigation of cavity shape.

Shape	A_R [-]	h_c in μm	w_c in μm	α in %
Rectangular, conical, spherical	0.01; 0.1; 1.0	1	10; 25; 50; 100; 150; 200	5; 10; 15; 20; 25; 30; 40

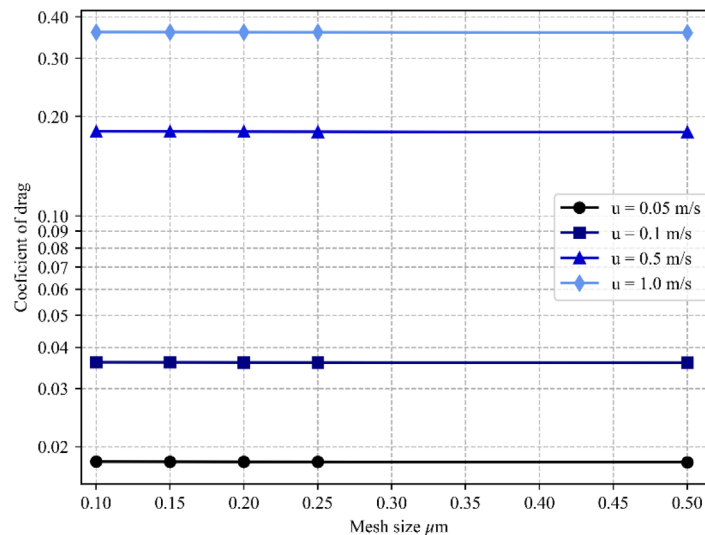


Fig. 5. Mesh independence for a spherical micro dimple textured surface. ($h = 30 \mu\text{m}$, $w_c = 10 \mu\text{m}$, $d_c = 5 \mu\text{m}$).

The procedure is comparable to that presented for the simulation and allows a qualitative comparison of the data. This procedure is chosen because it eliminates the effect of surface irregularities and imperfections of real surfaces, which can only be implemented in simulations at great

expense through relative comparison. Applying the equation to the experimentally recorded data yields the relative changes in COF shown in Figure 6d. On average, it is evident that the majority of tests lead to a reduction in the coefficient of friction. The only exceptions are the LT_{25}

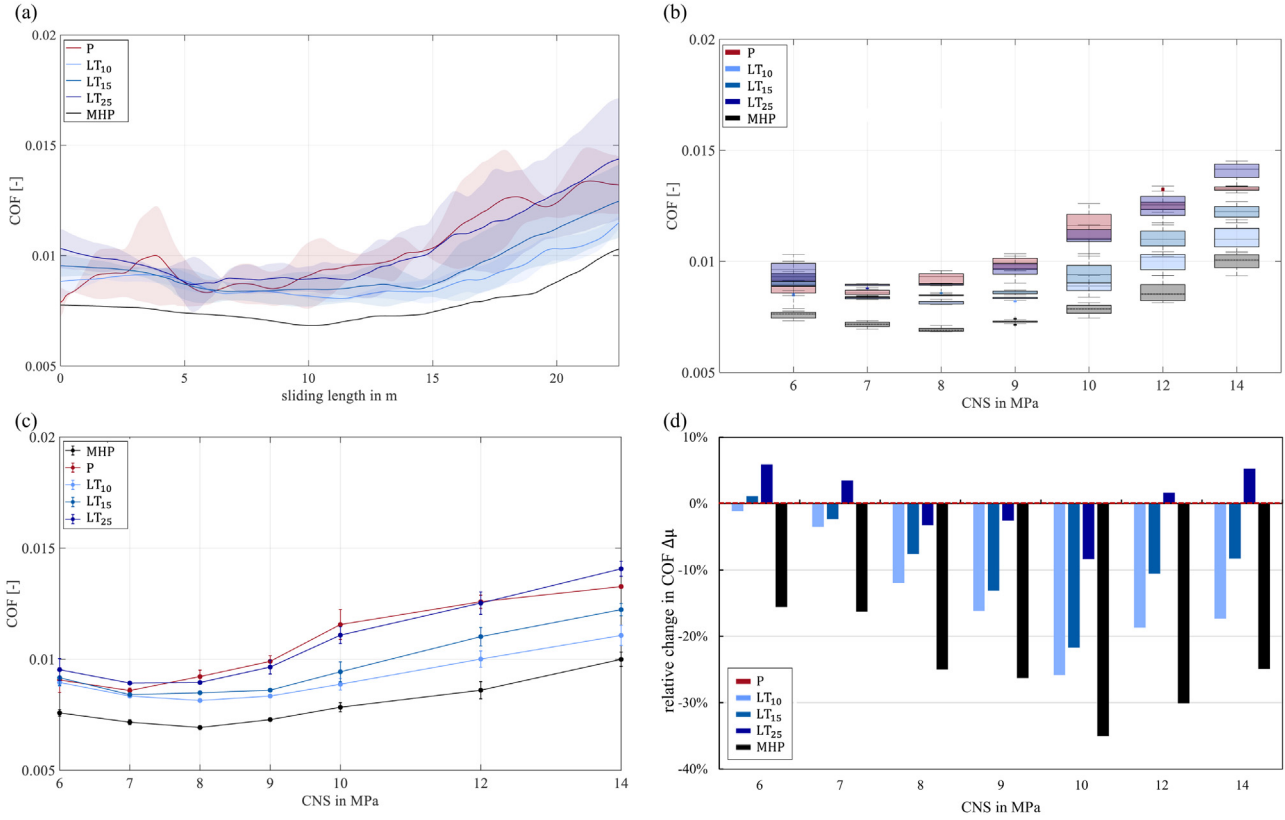


Fig. 6. (a) COF for the investigated specimen, (b) boxchart for constant pressure states, (c) evolution and error of COF for constant pressure states and (d) relative change in COF for constant pressure states.

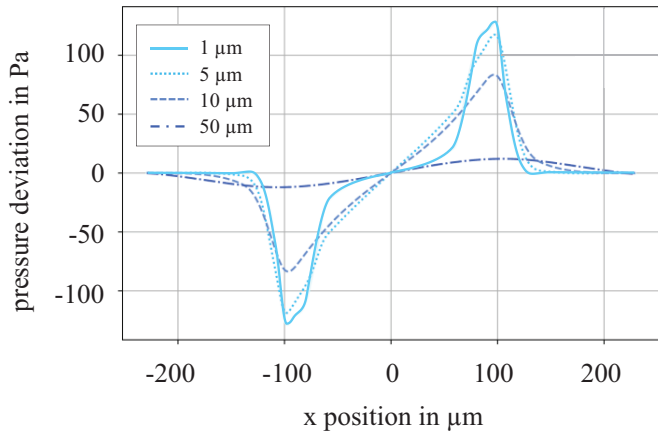


Fig. 7. Pressure deviation for varying lubrication clearances shown for $w_c = 200 \mu\text{m}$ and $\alpha = 30\%$.

coefficients, which are higher than those of the polished reference tools. Laser-textured dies, with α of 10% and 15% lead to a decrease in COF. However, a coverage of 25% eventually leads to an increase in COF for higher pressure levels. It can also be seen that 10% coverage contributes to the most significant reduction for the LT specimen. The local minimum is -26% at 10 MPa, and the reduction decreases further for higher CNS. The MHP textured specimen with 20% coverage displays an analogous pattern

of friction reduction with increasing CNS, with a local minimum at 12 MPa. Despite the significantly higher coverage compared to the optimum for laser-textured tools, a 34% reduction in COF can be achieved.

4.2 Correlation of lubrication clearance and pressure

Experimental findings show that increasing contact normal stresses (CNS) initially have a positive effect on friction-reducing properties [23]. To simulate the effect of increasing CNS, the lubrication clearance h_c was varied in the simulation model in five steps as a directly corresponding geometric variable. Figure 7 shows the resulting pressure distribution profiles along the x- coordinate (see Fig. 4) for a constant surface coverage of $\alpha = 30\%$ and a cavity width $w_c = 200 \mu\text{m}$. The absolute magnitude of pressure is found to be considerably influenced by the lubrication clearance. Reducing the lubrication clearance from $50 \mu\text{m}$ to $1 \mu\text{m}$ increases the absolute pressure by 622%. The relative movement is induced by the upper part of the tool. A reduction in lubrication clearance leads to higher velocity gradients, and therefore, a denser kinetic potential. Consequently, more kinetic energy is transmitted to the dimples via the lubricant.

Similarly to what Liu et al. [38] observed, under high kinetic energy, the lubricant is more susceptible to generating turbulence, thereby increasing the resulting pressure. This phenomenon is partially supported by experimental tribological studies. Here an increase in the

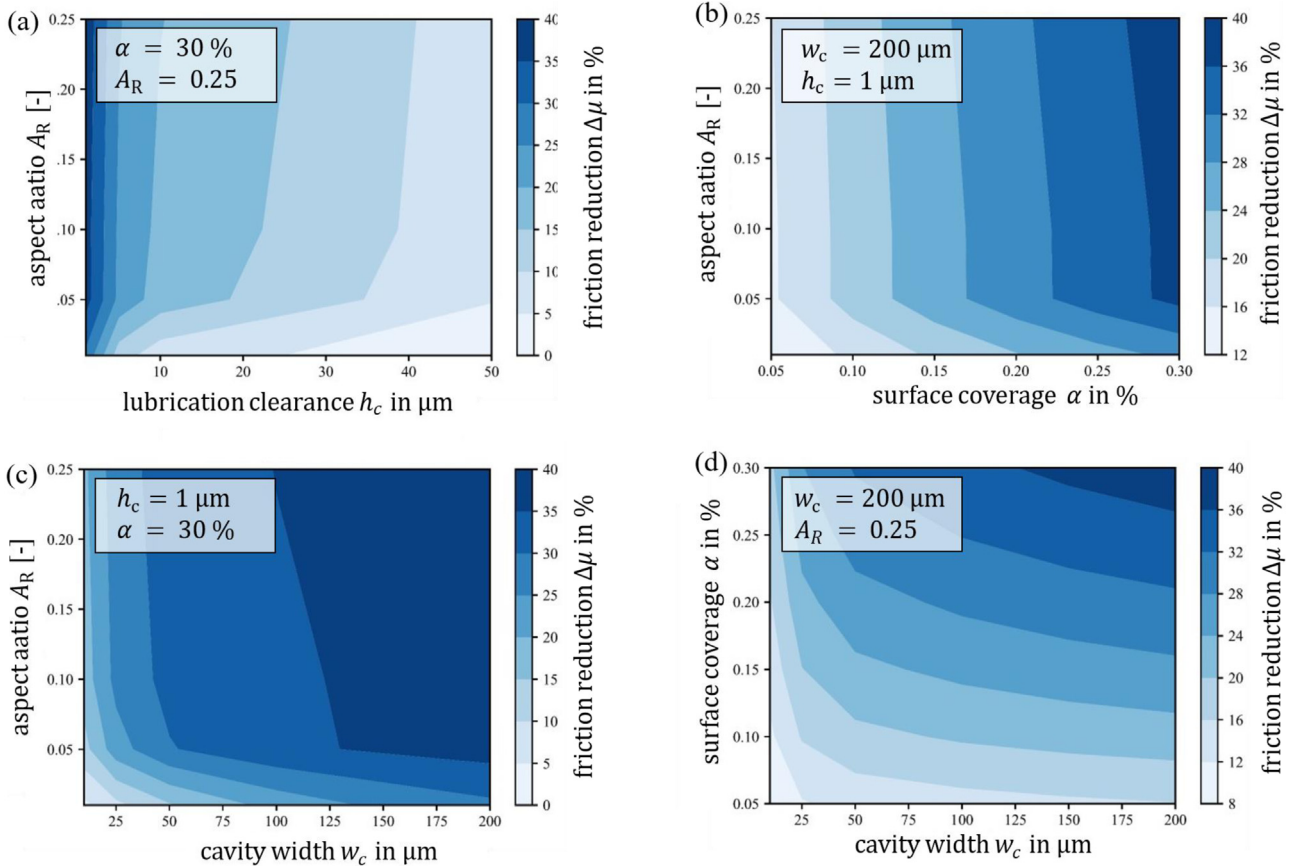


Fig. 8. Resulting friction reduction based on the simulation results for varying (a) aspect ratio A_R and lubrication clearance h_c ; (b) aspect ratio A_R and surface coverage α ; (c) aspect ratio A_R and cavity width w_c and (d) surface coverage α and cavity width w_c .

applied CNS, equivalent to the external load, contributes to an increase in the friction reducing properties for an incremental CNS increase of 6 up to 12 MPa. However, the pressure profiles of the simulation data do not support the sudden increase in friction as observed by Schumann et al. [23], with a further increase in CNS or respectively decreasing lubrication clearances.

4.3 Parameters affecting friction reduction

The pressure profiles shown in Figure 7 illustrate the resulting phenomena caused by the modified flow conditions, which in turn are caused by the geometric adjustments. To assess the impact on tribological properties, the resulting relative friction reduction is calculated using the parameters introduced (Sec. 3.4). As demonstrated in Figure 8, the outcoming results of varying the parameters and evaluating the coefficient of friction are presented using characteristic field diagrams. In each instance, two parameters were fixed at constant values. The following investigations consider the parameter variations listed in Table 4.

4.3.1 Effect of aspect ratio

The influence of the lubrication clearance and the simulative transfer on the friction-reducing properties is visualised in Figure 8a in the context of the aspect ratio A_R .

Notable effects on the friction reduction μ can only be observed for a lubrication clearance of less than $h_c = 10 \mu\text{m}$. Therefore, the minimum lubrication clearance of $h_c = 1 \mu\text{m}$ was assumed for the visualisation in all subfigures. As shown in Figure 8b, the aspect ratio and surface area are interdependent, with a low aspect ratio A_R having a negative effect on the friction reduction μ achievable for a constant surface coverage α . Above an aspect ratio of $A_R = 0.05$, the observed correlations are approximately linear. The same applies in the context of the cavity width w_c (Fig. 8c). Especially for a cavity width below $w_c = 75 \mu\text{m}$ the correlation is almost linear. The results indicate that high aspect ratios prove advantageous in achieving optimum friction reduction. Within the scope of the parameter variation considered, it can be concluded that the minimum friction reduction is achieved at low aspect ratios, low coverage ratios and low cavity widths. However, compared to an untextured surface, an enhancement of approximately $\Delta\mu = 10\%$ is still observed. The most substantial reduction is attained in the opposite direction.

4.3.2 Effect of cavity width

Figure 8d demonstrates the variation of cavity width w_c in correlation with surface coverage α that cavity widths of less than $w_c = 75 \mu\text{m}$ only result in a marginal decrease in the friction coefficient as the coverage ratio increases.

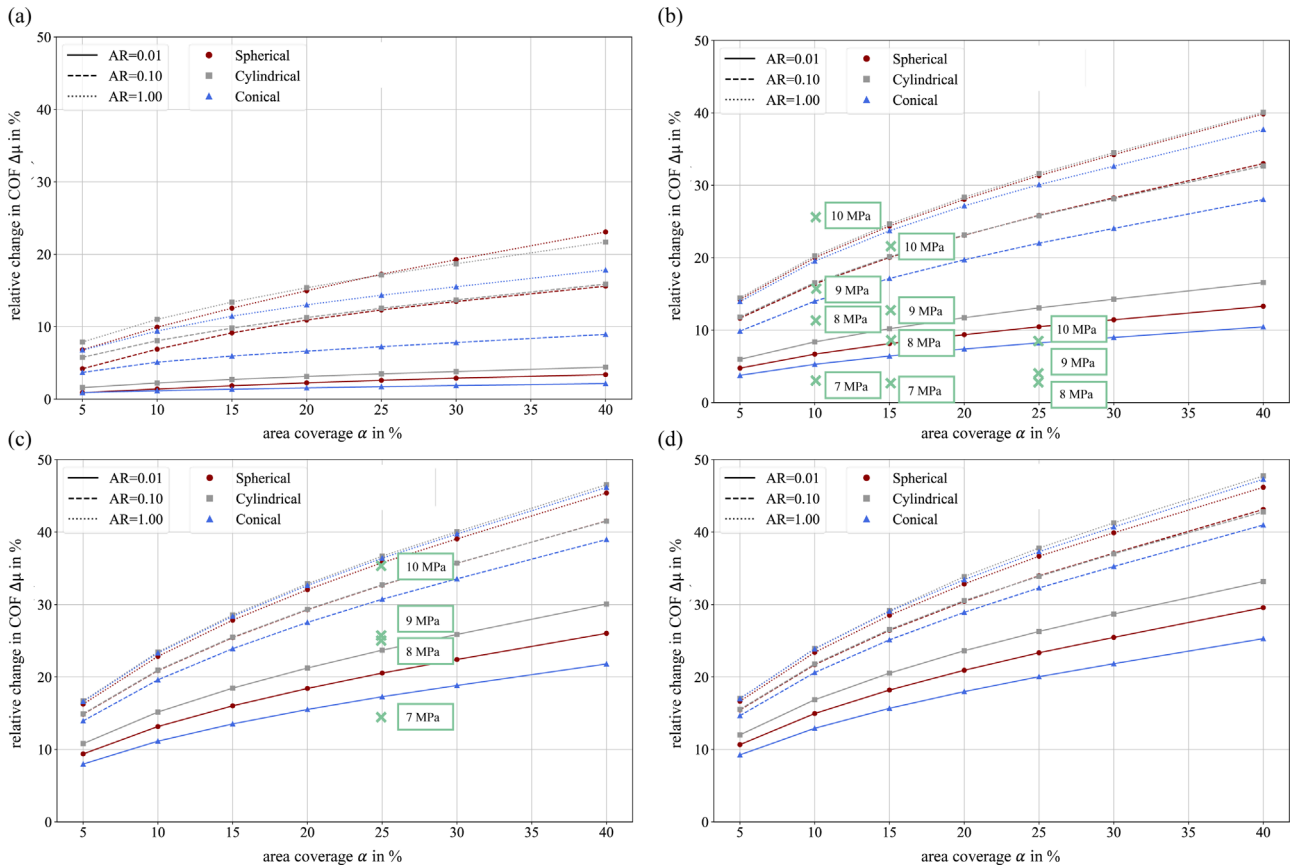


Fig. 9. Effect of cavity shape and aspect ratio on change in COF for (a) $w_c = 10\mu\text{m}$, (b) $w_c = 50\mu\text{m}$, (c) $w_c = 150\mu\text{m}$ and (d) $w_c = 200\mu\text{m}$. Turquoise crosses indicate experimental data for specific coverage ratios and CNS.

For instance, with a cavity width of approximately $w_c = 25\mu\text{m}$ and a coverage ratio of $\alpha = 20\%$, a friction reduction of $\mu = 16\%$ is attained, whereas a cavity width of $w_c = 125\mu\text{m}$ causes a friction reduction of $\mu = 24\%$. This observation is consistent with the experimental findings reported in the literature on the operating field in consideration. In the context of laser-textured tools with a smaller cavity width, a lower reduction in friction was observed compared to tools textured by MHP with a larger cavity width, for an equivalent coverage ratio. The maximum magnitude of friction reduction observed experimentally is $\mu = 18\%$ for laser textured specimens and $\mu = 31\%$ for textured tools by MHP. The simulated results thus show a high degree of agreement with the experimental observations [23]. The correlations are discussed in further detail in Section 4.3.4.

4.3.3 Effect of coverage ratio

The simulated observations in Figure 8b and Figure 8d suggest that an increase in coverage ratio α has a positive effect on the reduction of friction in the context of both aspect ratio and cavity width. For the parameter set under investigation, the simulations indicate that a maximum friction reduction of approximately $\mu = 40\%$ can be attained at coverage ratios exceeding $\alpha = 25\%$, independent of the aspect ratio A_R . This observation is consistent with the theoretical framework proposed by Uehara et al. [22],

which attributes the reduction in friction to the enhanced lubricant entrainment and pressure generation facilitated by an increasing number of surface cavities. However, both theoretical and experimental studies have consistently reported the existence of threshold effect: while moderate increases in coverage ratio improve the beneficial effects of lubrication, values beyond a critical range may diminish the benefits. Specifically, excessive coverage ratios have been associated with reduced load carrying capacity, instability of lubricant films, and localized lubricant starvation leading to a change in lubrication regime, ultimately increasing friction. [20,23,40].

4.3.4 Effect of cavity shape

By simulating different cavity shapes, the effects of shape, dimension characteristics, and the influence of aspect ratio can be objectively evaluated (see Tab. 5). Figure 9 represents these effects. Here, different cavity widths w_c are plotted in (a)-(d) with variations in the coverage ratio, and the influence on the relative change in the coefficient of friction is plotted. In general, the results show that the reduction in the COF increases with increasing coverage ratio α . This is consistent with the previously shown figures. From an α value of 25% onwards, the increase is approximately linear. When considering the influence of the aspect ratio A_R of the cavities, it is also apparent that an increase in size leads to greater friction reduction. Using

spherical cavities as an example for an aspect ratio of $A_R = 0.1$ and $\alpha = 20\%$ the reduction by 11%, 20%, and 22% increases for w_c 50 to 200 μm , when compared to the initial 12%. The influence of shape is also of interest. Contrary to expectations, across all simulated results, rectangular geometries with a constant aspect ratio and coverage ratio lead to the highest reduction, while conical shapes are the least effective. This is consistent with the experimental observations. The experimental results showed a more significant friction reduction for spherical cavities. The aspect ratio has the most significant effect. The logarithmic increase in aspect ratio thus leads, in the case of rectangular geometries with a width of $w_c = 150 \mu\text{m}$, to an increase of 21% for $A_R = 0.1$ and 26% for $A_R = 1.0$, compared to $A_R = 0.01$ for $\alpha = 15\%$. Therefore, it can be pointed out that, according to the simulation results, particularly wide textures with a high aspect ratio should be aimed for. However, the technical feasibility of production must be taken into account here. The limitations for spherical geometries are $A_R = 0.4$. If the value exceeds 0.4, the width of the cavity w_c decreases relative to the depth d_c . The maximum diameter of the spherical cavity is therefore below the surface. These geometries cannot be produced using conventional subtractive or forming manufacturing methods.

Figure 9b shows the experimentally recorded data for the tools produced by LT. The relative friction changes achieved for the different coverage ratios for the CNS under consideration are marked with crosses. The same was done in Figure 9c for the spherical textures. The comparison shows that LT achieves a good approximation for a CNS of 9 MPa in the case of $\alpha = 10\%$. Simulations show a friction reduction $|\mu| = 14\%$, while experimental data show $|\mu| = 16\%$. A more significant deviation is observed at 8 MPa $|\mu| = 12\%$ and eventually decreased up to $|\mu| = 3\%$ for 7 MPa. For larger coverage ratios, the data is significantly underestimated. It is particularly noticeable here that the experimentally observed decrease in relative friction change is not reflected. Experimentally, phenomena appear to come into effect here that are not reflected by the assumptions defined in the simulation. Possible explanations include the quality and reproducibility of the cavities generated by the nanosecond laser. Firstly, there is a wide variation in cavity width w_c and, in particular, cavity depth d_c (see Tab. 2). In addition, the cavity ground shows asperities due to the manufacturing process and the solidification of material, while the simulation considers smooth ground. Within experiments, this potentially contributes to undesirable flow effects. This effect scales with the increasing number of cavities and, respectively, the coverage ratio. It reduces the effective load-bearing capacity, resulting in a state of limit and mixed friction being reached more quickly. Conversely, an overestimation is observed for spherical cavities, in contrast to the data generated by experimentation. (see Fig. 9c). For the coverage ratio considered experimentally, the change in COF $|\mu|$ equals 25% for CNS of 8 MPa, and 26% for CNS of 9 MPa. The simulated result indicates $|\mu| = 21.5\%$ in comparison. However, the deviation is similar to that discussed for conical cavities and describes a good approximation. Possible explanations for the deviation

are that the textures have a direct influence on the lubricating film thickness formed. This cannot be quantified in the experimental setup used (see Fig. 1). The results shown in Section 4.2 clearly demonstrate that the influence of lubrication clearance h_c and thus, experimentally, the lubricating film thickness is significant. A geometric increase in h_c would directly contribute to a lower change in $|\mu|$, and therefore increase the agreement between simulation and experiment. Another explanation for the derivation is the design of the inlet and outlet of the cavity. While the chosen geometric definition in the simulation model generates a comparatively sharp edge at the inlet and outlet for spherical geometries, the structures generated by MHP have a very smooth transition from the initial surface to the cavity. The fluid mechanical influence of these cavities is evident when comparing rectangular and spherical cavities. As already discussed, rectangular-shaped geometries always have a higher friction reduction than their spherical counterparts. Inlet and outlet edges are particularly sharp here. Overall, it can be concluded that LT₁₀ and MHP show satisfactory agreement with the simulated data for CNS in the range of 8–9 MPa, thereby verifying the model as satisfactory.

In addition, as discussed previously, it should be noted that the assumptions of the simulation model have some limitations and do not reflect real effects such as possible plastic flow of the material into the cavity, which contributes to mechanical anchoring. This is not depicted in the simulation. Similarly, volatilisation of the lubricant and increasing thinning due to phenomena such as real contact normal stress as described by Uehara et al, are also ignored [22]. An increasing reduction in channel height h_c due to physical phenomena is not implemented. This effect could not be reproduced in the simulations. This is because the simulation model assumes ideal, smooth surfaces with no elasticity, meaning mixed and boundary lubrication are not taken into account. Due to the model assumptions of a rigid channel, volatilisation of the fluid due to increasing external load is not represented. This is critical for the transition from hydrodynamic to mixed friction. Experimentally, once a system-dependent threshold is exceeded, the lubricant film becomes sufficiently thin, such that surface roughness or elastic deformations of the material cause contact between the friction bodies. In Uehara's theory, this corresponds to the effect of the effective contact normal stress. To model this phenomenon, kinematic or elastic simulation models coupled with finite element analysis (FEA) or FSI models would be required. This would involve considerably more complex modelling steps and computing costs and is therefore beyond the scope of this work. Effects such as initial wetting or flooding of the cavities are also not considered in the simulation. These effects are particularly significant in cases of large aspect ratios or high viscosities, as investigated by Shimizu et al [41]. Ultimately, this means that no increase in COF can be observed for the varied increasing parameters in the results of the simulation based purely on fluid mechanics, since the transition from hydrodynamic lubrication to mixed or boundary friction is depicted.

5 Conclusion

In this study, surface texture dimensioning was approached through a two-dimensional modelling framework. Three-dimensional geometrical variables were abstracted into two-dimensional space by several simplifying assumptions. Despite this projection, the simulations demonstrated a high degree of agreement with experimental observations. The numerical results were able to quantitatively reproduce the relative change in the coefficient of friction while taking different cavity shapes into account. In combination with the theoretical and experimental contributions of Shimizu et al. [41] and Bay et al. [42] regarding lubricant volatilisation and wetting phenomena, the findings of this work provide a significant extension to the scientific understanding of tribological mechanisms of textures in sheet metal forming. From an application perspective, the potential impact of this research lies in reducing frictional losses, thereby contributing to improved energy and resource efficiency in industrial forming processes. The principal findings can be summarized as:

- A geometric reduction in the lubricating clearance adequately models the phenomena of increasing normal contact pressure up to a certain extent.
- Consistent with experimental findings, the most pronounced friction reduction is achieved under conditions of reduced lubrication clearance.
- The simulated geometric abstractions of coverage ratio are consistent with experimentally observed behavior under varying tribological load conditions.
- The theoretical prediction of friction reduction with increasing number of cavities is supported numerically.
- Among the investigated parameters, the aspect ratio A_R and cavity width w_c take the most significant influence on cavity design.

The procedure presented in this study provides an effective framework for designing the cavity geometries and coverage ratios tailored to unidirectional lubricant flow in the micrometre range. This constitutes a fundamental basis for systematic geometric optimization of cavities and coverage ratios in sheet metal forming processes characterized by varying load spectra and unidirectional relative motion under hydrodynamic lubrication.

However, certain modelling simplifications are assumed. Due to the neglect of die elasticity, sheet plasticity, an incompressible fluid, and the assumption of an ideally smooth microscopic surface, the present approach is not capable of capturing multiscale flow effects or regimes involving mixed or boundary lubrication. Future developments of the method will therefore focus on the coupling of elastic and plastic deformation models, enabling the superposition of structural with fluid mechanics. This extension will allow the framework to represent additional lubrication regimes with greater fidelity.

Subsequent research should pay particular attention to the detailed investigation of inlet and outlet geometries, as well as wetting probabilities, since these factors have a significant impact on the initiation and stability of lubrication mechanisms. Incorporating these aspects will

enable the procedure to capture a much broader spectrum of tribological phenomena relevant to forming technology. This is significant for improving our understanding of complex mechanisms in sheet metal forming processes such as microplastic hydrodynamic lubrication.

Acknowledgments

The presented results are part of the research project “Tribomized Sheets” of the European Research Association for Sheet Metal Working (EFB) as well as all participating companies for their support in the project. The authors also would like to thank the assisting students Kadambi R. Krishna, Harsha V. Aluri, Manikanteswar R. Goluguri and Karangula P. Reddy for their support in the numerical simulations.

Funding

The authors would like to thank the German Aerospace Center (Deutsches Zentrum für Luft- und Raumfahrt, DLR) and the German Federal Ministry for Economic Affairs and Climate Action (Bundesministerium für Wirtschaft und Klimaschutz, BMWK) for funding within the framework of project no. IGF 01FI23445N.

Conflicts of interest

The authors have nothing to disclose.

Data availability statement

The data is proprietary to the Institute for Production Engineering and Forming Machines – PtU Research and cannot be made publicly available. Nonetheless, the authors are willing to share selected datasets with qualified researchers upon reasonable request and subject to institutional approval.

Author contribution statement

Conceptualization: Philipp Schumann, Daniel Martin; **Methodology:** Philipp Schumann; **Software:** Otavio Serra **Validation:** Philipp Schumann, Daniel Martin; **Formal Analysis:** Philipp Schumann, Daniel Martin; **Investigation:** Philipp Schumann, Daniel Martin; **Resources:** Philipp Schumann, Daniel Martin; **Data Curation:** Philipp Schumann, Daniel Martin; **Writing – Original Draft Preparation:** Philipp Schumann **Writing – Review & Editing:** Philipp Schumann, Daniel Martin, Peter Groche; **Visualization:** Philipp Schumann, Daniel Martin, Mano Raja; **Supervision:** Peter Groche; **Project Administration:** Philipp Schumann, Peter Groche; **Funding Acquisition:** Peter Groche.

References

1. H. Hegab, N. Khanna, N. Monib, A. Salem, Design for sustainable additive manufacturing: a review, *Sustain. Mater. Technol.* **35** (2023) e00576
2. T. Kober, H.-W. Schiffer, M. Densing, E. Panos, Global energy perspectives to 2060-WEC’s World Energy Scenarios 2019, *Energy Strategy Rev.* **31** (2020) 100523

3. W.N. Ryerson, Population: the multiplier of everything else, in: The post carbon reader: Managing the 21st century's sustainability crises, 2010, pp. 153–175
4. Z. Wu, T.S. Adebayo, A.A. Alola, Renewable energy intensity and efficiency of fossil energy fuels in the nordics: how environmentally efficient is the energy mix?, *J. Clean. Prod.* **438** (2024) 140711
5. J.L. Holecek, H.M.E. Geli, M.N. Sawalhah, R. Valdez, A global assessment: can renewable energy replace fossil fuels by 2050?, *Sustainability* **14** (2022) 4792
6. K. Holmberg, A. Erdemir, Influence of tribology on global energy consumption, costs and emissions, *Friction* **5** (2017) 263–284
7. W. Colglazier, Sustainable development agenda: 2030, *Science (New York, N.Y.)* **349** (2015) 1048–1050
8. D. Bowman, G. van Calster, Reflecting on REACH: Global implications of the European Union's chemicals regulation, *Nanotech. L. Bus.* **4** (2007) 375
9. A. Feroq, S. Lamouri, V. Carbone, Lean/Green integration focused on waste reduction techniques, *J. Clean. Prod.* **137** (2016) 567–578
10. S. Bahadur, The economic impact of wear on society, 0022-2305, **100** (1978) 145–147
11. T. Trzepieciniski, Recent developments and trends in sheet metal forming, *Metals* **10** (2020) 779
12. M. Woydt, The importance of tribology for reducing CO₂ emissions and for sustainability, *Wear* **474** (2021) 203768
13. Y. Lu, M. Hua, Z. Liu, The biomimetic shark skin optimization design method for improving lubrication effect of engineering surface, *J. Tribol.* **136** (2014) 31703
14. M. Yang, S. Evans, Rapid decarbonization requires industrial efficiency, *Nat. Rev. Clean Technol.* **1** (2025) 4–5
15. D. Patel, V.K. Jain, J. Ramkumar, Micro texturing on metallic surfaces: State of the art, *Proc. Inst. Mech. Eng. Part B: J. Eng. Manuf.* **232** (2018) 941–964
16. V. Sharma, P.M. Pandey, Recent advances in turning with textured cutting tools: a review, *J. Clean. Prod.* **137** (2016) 701–715
17. J. Hazrati, P. Stein, P. Kramer, A.H. van den Boogaard, Tool texturing for deep drawing applications, in: IOP conference series: materials science and engineering, (2018) p. 12095
18. T. Shimizu, H. Kan, H. Messaoudi, F. Vollertsen, M. Yang, Impact of geometrical parameters of micro-textured DLC on tribological properties under dry sliding friction, *Manuf. Rev.* **6** (2019) 18
19. K. Kitamura, T. Makino, M. Nawa, S. Miyata, Tribological effects of punch with micro-dimples in blanking under high hydrostatic pressure, *CIRP Annals* **65** (2016) 249–252
20. P. Schumann, V. Arne, P. Groche, Improved tribological properties of blanking punches for copper alloys utilizing deterministic surface texturing by machine hammer peening, *Coatings* **15** (2025) 136
21. P. Kersting et al., Experimental and numerical analysis of tribological effective surfaces for forming tools in sheet-bulk metal forming, *Prod. Eng.* **10** (2016) 37–50
22. Y. Uehara, M. Wakuda, Y. Yamauchi, S. Kanzaki, S. Sakaguchi, Tribological properties of dimpled silicon nitride under oil lubrication, *J. Eur. Ceram. Soc.* **24** (2004) 369–373
23. P. Schumann, P. Groche, R. Lindner, Influence of different deterministic surface texturing processes on friction and tool life for load collectives in sheet metal forming, in: *Proceedings: Tribology International Conference 2023*, 2023
24. E. Ciulli, Tribology and sustainable development goals, in: G. Quaglia, A. Gasparetto, V. Petuya, G. Carbone (Eds.), *Mechanisms and Machine Science, Proceedings of I4SDG Workshop 2021*, Springer International Publishing, Cham 2022, pp. 438–447
25. W. Liu, H. Ni, P. Wang, H. Chen, Investigation on the tribological performance of micro-dimples textured surface combined with longitudinal or transverse vibration under hydrodynamic lubrication, *Int. J. Mech. Sci.* **174** (2020) 105474
26. M. Tošić, R. Larsson, J. Jovanović, T. Lohner, M. Björling, K. Stahl, A computational fluid dynamics study on shearing mechanisms in thermal elastohydrodynamic line contacts, *Lubricants* **7** (2019) 69
27. Y. Carretta, R. Boman, J. Bech, N. Legrand, M. Laugier, J.-P. Ponthot, Numerical modelling of microscopic lubricant flow in sheet metal forming. Application to plane strip drawing, *Int. J. Numer. Methods Eng.* **112** (2017) 203–237
28. P. Schumann, D. Martin, O.M. Serra, P. Groche, Cavity design for surface textured sheets in metal forming, *MATEC Web Conf.* (2025) 1053
29. P. Groche, N. Moeller, H. Hoffmann, J. Suh, Influence of gliding speed and contact pressure on the wear of forming tools, *Wear* **271** (2011) 2570–2578
30. P. Groche, M. Christiany, Y. Wu, Load-dependent wear in sheet metal forming, *Wear* **422** (2019) 252–260
31. M. Christiany, P. Groche, Reproducibility of wear tests and the effect of load on tool life in sheet metal forming, *AMR* **1018** (2014) 293–300
32. D. Yu, D. Cao, Z. Li, Q. Li, Experimental and CFD studies on the effects of surface texture on liquid thickness, wetted area and mass transfer in wave-like structured packings, *Chem. Eng. Res. Des.* **129** (2018) 170–181
33. G. Caramia, G. Carbone, P. de Palma, Hydrodynamic lubrication of micro-textured surfaces: two dimensional CFD-analysis, *Tribol. Int.* **88** (2015) 162–169
34. J. Han, L. Fang, J. Sun, S. Ge, Hydrodynamic lubrication of microdimple textured surface using three-dimensional CFD, *Tribol. Trans.* **53** (2010) 860–870
35. M. Ludwig, C. Müller, P. Groche, Simulation of dynamic lubricant effects in sheet metal forming processes, *Key Eng. Mater.* **438** (2010) 171–178
36. B. LotfizadehDehkordi, P.J. Shiller, G.L. Doll, Pressure-and temperature-dependent viscosity measurements of lubricants with polymeric viscosity modifiers, *Front. Mech. Eng.* **5** (2019) 18
37. N. Marx, L. Fernández, F. Barceló, H. Spikes, Shear thinning and hydrodynamic friction of viscosity modifier-containing oils. Part I: shear thinning behaviour, *Tribol. Lett.* **66** (2018) 92
38. W. Liu, H. Ni, H. Chen, P. Wang, Numerical simulation and experimental investigation on tribological performance of micro-dimples textured surface under hydrodynamic lubrication, *Int. J. Mech. Sci.* **163** (2019) 105095

39. T.S. Yang, Investigation of the strain distribution with lubrication during the deep drawing process, *Tribol. Int.* **43** (2010) 1104–1112
40. M. Steitz, P. Stein, P. Groche, Influence of hammer-peened surface textures on friction behavior, *Tribol. Lett.* **58** (2015), <https://doi.org/10.1007/s11249-015-0502-9>
41. Shimizu, Kobayashi, Vorholt, Yang, Lubrication analysis of micro-dimple textured die surface by direct observation of contact interface in sheet metal forming, *Metals* **9** (2019) 917
42. J. Bech, N. Bay, M. Eriksen, Entrapment and escape of liquid lubricant in metal forming, *Wear* **232** (1999) 134–139

Cite this article as: Philipp Schumann, Daniel Martin, Otavio Moro Serra, Mano Prithvi Raj Raja, Peter Groche, Effect of cavity design on textured tool surfaces in sheet metal forming, *Manufacturing Rev.* **12**, 27 (2025), <https://doi.org/10.1051/mfreview/2025024>